



# A Real-Time Supervisory Control Strategy for Roll-to-Roll Dry Transfer of 2D Materials and **Printed Electronics**

Qishen Zhao , Christopher Martin, Nan Hong, Member, IEEE, Dongmei Chen , Member, IEEE, and Wei Li

Abstract—With the advancement of manufacturing technology in transfer printing and two-dimensional materials fabrication, roll-to-roll (R2R) dry transfer by mechanical peeling is becoming a promising process for efficient transfer of thin film materials from a donor substrate to a target substrate for device fabrication. As a key process variable, the peeling angle determines the loading condition of the R2R dry transfer process and thus the quality of the transferred material. Controlling the peeling angle is challenging in a R2R process because of the adhesion energy and peeling front velocity in addition to the flexible substrates involved in the peeling process. In this article, a real-time supervisory control strategy is developed for the R2R mechanical peeling process. A strain energy-based peeling process model is employed to estimate the peeling front velocity and the adhesion energy. The real-time estimation is then used to generate reference signals for web tension controllers to track the desired peeling angles. The proposed control strategy is demonstrated with both simulation and experimental results.

Index Terms—Real-time supervisory control, roll-to-roll (R2R) manufacturing process control, transfer printing, two-dimensional (2-D) materials fabrication.

#### I. Introduction

R OLL-TO-ROLL (R2R) manufacturing is a high-throughput method to produce a variety of advanced products, such as flexible and stretchable electronics [1], [2], [3], [4], lithium-ion battery electrodes [5], [6], solar cells [7], [8], [9], and other system-in-foil devices [10]. As the technology develops, R2R dry transfer by mechanical peeling is becoming a promising process to transfer two-dimensional (2-D) materials [11], [12], [13], [14], [15] and printed electronics [16], [17],

Manuscript received 28 August 2022; revised 6 December 2022; accepted 27 January 2023. Date of publication 28 February 2023; date of current version 17 October 2023. This work was supported by the National Science Foundation under Cooperative Agreement EEC-1160494 and CMMI-2041470. Recommended by Technical Editor C. E. Okwudire. (Corresponding authors: Dongmei Chen; Wei Li.)

The authors are with the Walker Department of Mechanical Engineering, University of Texas, Austin, TX 78712 USA (e-mail: qishenzhao0904@utexas.edu; cbmartin129@utexas.edu; nan1995@ utexas.edu; dmchen@me.utexas.edu; weiwli@austin.utexas.edu).

Color versions of one or more figures in this article are available at https://doi.org/10.1109/TMECH.2023.3243123.

Digital Object Identifier 10.1109/TMECH.2023.3243123

[18], [19], [20] from one substrate to another for device fabrication. R2R device transfer is a critical manufacturing step, as many 2-D materials and flexible electronics must be fabricated on substrates that are not suited for product end-use. R2R mechanical peeling has recently been proposed for transferring 2-D materials due to its advantages over other methods such as wet etching and electrochemical delamination [11], [21], [22], [23], [24]. The dry transfer method is fast, does not introduce chemical contamination, and allows for the recycling of the metal substrate that the 2-D material is grown on. Meanwhile, a polymeric stamp has been used to pick up components or patterns fabricated on a donor substrate and transfer them onto a target substrate for transfer printing electronics [16]. We anticipate that the R2R dry transfer method can be expanded to replace the discrete stamp process, which is also a mechanical peeling process, and facilitate a continuous high-throughput transfer process for printed electronics.

Mechanical peeling has been studied previously in a batch mode, using manual or semiautomated setups where a flexible film was peeled from a rigid substrate. It has been shown that the web speed and peeling front geometry, characterized by peeling angles, are critical to ensuring successful transfer [11], [12], [15]. Also, in the stamp-based transfer printing process for flexible electronics, some stamps are designed such that the mechanical adhesion between the stamp and the materials to be transferred can be modulated with the peeling angle [20]. Bending radius of the substate during the mechanical peeling process, which is another way of characterizing the peeling angle, is also shown to be effective in switching between the pick and place modes in the transfer printing process [18].

Compared with conventional manual and semiautomated batch-mode operations, R2R mechanical peeling presents a significant challenge to peeling angle control due to the complex interactions between the two flexible substrates and the roller system dynamics. The peeling angle is affected by both the peeling front velocity and the adhesion energy between the donor substrate and the material to be transferred. The web tensions during the peeling process need to satisfy a certain criterion to ensure successful peeling. Recently, a strain energy-based peeling process model was developed to characterize the relationship between the peeling angles and process parameters such as adhesion energy, roller speed, peeling front velocity, and web tension

in the R2R dry transfer system [23]. While the model is shown capable of capturing the transient behavior the R2R mechanical peeling process, a method to directly control the peeling angles by employing this model has not been demonstrated.

In this article, we propose a real-time supervisory control strategy to control the peeling angles in the R2R mechanical peeling process. To our knowledge, this is the first published attempt to control the peeling angles directly in a R2R mechanical peeling system. Most previous studies on mechanical peeling have focused on material properties or process parameters as opposed to controls. Studies focusing on R2R system controls dealt with web speed and tension tracking exclusively, such as those for tape transfer and web processing lines [25], [26]. Peeling angle control is different, as in peeling angle controls, multiple web tension zones are coupled together at the peeling front and the angles are affected by tensions on multiple webs. In addition, an accurate estimation of the adhesion energy between the flexible webs is necessary to accurately control the peeling angles in R2R dry transfer.

The control framework presented in this article consists of a high-level supervisory controller and two regulatory-level tension controllers. The supervisory controller employs the peeling process model to generate reference tension signals in real-time that, based on the estimated adhesion energy and peeling front velocity, will result in the desired peeling angles. The tension reference will then be used in tension tracking control, where a dynamic feedforward control is integrated with a feedback control [27]. The proposed control strategy is validated with simulation and experimental results from a custom-built R2R dry transfer testbed.

### II. R2R PEELING SYSTEM ANALYSIS

# A. R2R Peeling System Model

Figure 1 shows a schematic of the R2R mechanical peeling process [23]. A roll of laminated web on an unwinding roller is fed into the system and peeled after two idler nipping rollers of radius R, as shown in Fig. 1(a). The two peeled substrates are then collected by two rewinding rollers. The unwinding roller is controlled by a motor rotating at an angular velocity  $\omega_1$ . The linear unwinding speed is  $v_1$ . The two rewinding rollers are controlled by two motors providing torques  $u_2$  and  $u_3$ . The linear velocities of the webs at the two rewinding rollers are denoted as  $v_2$  and  $v_3$ . The three web sections separated by the peeling front form three tension zones and the tensions are denoted as  $t_1$ ,  $t_2$  and  $t_3$ , respectively. These three tensions are measured with tension roller loadcells denoted as  $LC_1$ ,  $LC_2$ , and  $LC_3$ , respectively. The peeling front geometry is described by two peeling angles:  $\theta$  and  $\alpha$ . The peeling front velocity, which is the speed of the peeled front propagation, is denoted as  $v_p$ .

During a stable peeling process, the energy released when generating a unit area of free interface will be the same as the adhesion energy of the interface, i.e.,

$$G = \Gamma \tag{1}$$

where G is the energy release rate of the peeling process and  $\Gamma$  is the adhesion energy, which is a property of an adhesive bond.

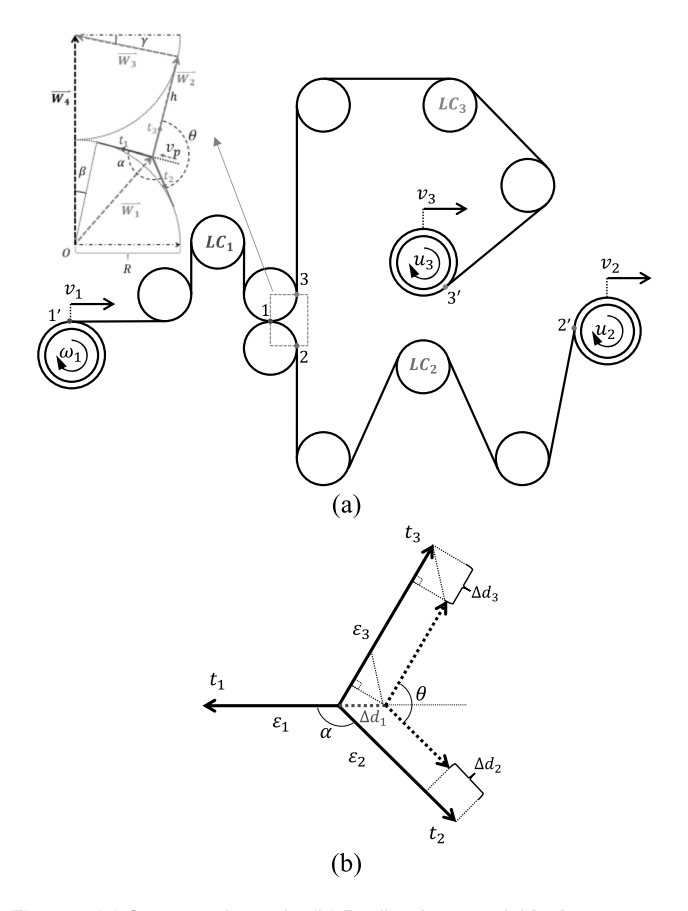


Fig. 1. (a) System schematic, (b) Peeling front model [23].

Given the peeling front geometry, the energy release rate G can be determined as [23], [28]

$$G = \frac{t_3}{b} \left( 1 + \cos\left(\theta + \alpha\right) + \varepsilon_3 + \varepsilon_1 \cos\left(\theta + \alpha\right) \right)$$

$$+ \frac{t_2}{b} \left( 1 + \cos\alpha + \varepsilon_2 + \varepsilon_1 \cos\alpha \right) - \frac{h_{w3} E_3}{2} \left( \varepsilon_3^2 - \varepsilon_1^2 \right)$$

$$- \frac{h_{w2} E_2}{2} \left( \varepsilon_2^2 - \varepsilon_1^2 \right) \tag{2}$$

where b is the width of the web,  $\varepsilon_1$ ,  $\varepsilon_2$ , and  $\varepsilon_3$  are elastic strains in the corresponding web sections,  $h_{w2}$  and  $h_{w3}$  are the web thicknesses, and  $E_2$  and  $E_3$  are the elastic moduli of web Sections II and III, respectively. The energy release rate expression can be obtained by analyzing the peeling system as in Fig. 1(b) where a crack with length of  $\Delta d$  is created. By considering the energy involved in the crack growth process, there are three categories of energy involved: the energy dissipated due to the new crack creation  $U_1$ , the potential energy changed by external force  $U_2$  and the elastic potential energy change  $U_3$ , as in (3)–(5). The sum of the three categories should be zero

$$U_1 = -\Gamma b \Delta d \tag{3}$$

$$U_2 = t_2 \Delta d_2 + t_3 \Delta d_3 \tag{4}$$

$$U_{3} = \frac{1}{2} E_{2} b h_{w2} \Delta d \left( \varepsilon_{1}^{2} - \varepsilon_{2}^{2} \right) + \frac{1}{2} E_{3} b h_{w3} \Delta d \left( \varepsilon_{1}^{2} - \varepsilon_{3}^{2} \right).$$
 (5)

Furthermore, the peeling angles  $\theta$  and  $\alpha$  can be determined by performing a force balance analysis among the three tensions:

$$\theta = \pi - \cos^{-1}\left(\frac{t_2^2 + t_3^2 - t_1^2}{2t_2t_3}\right) \tag{6}$$

$$\alpha = \pi - \cos^{-1}\left(\frac{t_1^2 + t_2^2 - t_3^2}{2t_1t_2}\right). \tag{7}$$

As the peeling front location moves, the web lengths on the three sides of the peeling front change as well. As shown in Fig. 1(a), the total length of each web section from the corresponding roller to the peeling front is [23]

$$L_1 = D_1 + R \cdot \beta + R \tan\left(\frac{\pi - \alpha}{2}\right) \tag{8}$$

$$L_2 = D_2 + R\left(\alpha - \frac{\pi}{2} - \beta\right) + R\tan\left(\frac{\pi - \alpha}{2}\right) \tag{9}$$

$$L_3 = D_3 + R\gamma + h. \tag{10}$$

where  $D_1$ ,  $D_2$ , and  $D_3$  are defined as the web lengths between the corresponding tangential points on the nipper rollers and the unwinding/rewinding rollers, e.g.,  $D_1$  is the web length between points I and I',  $\beta$  is the central angle corresponding to the arc section that the incoming laminate is wrapped around the lower nipping roller,  $\gamma$  is the central angle corresponding to the arc section that the upper web is wrapped around the upper nipping roller, and h is the web length between the peeling front and the tangential point on the upper roller. Additionally, based on the trigonometry relationship shown in the insert of Fig. 1(a),  $\vec{W}_1 + \vec{W}_2 + \vec{W}_3 = \vec{W}_4$ , where  $\vec{W}$ 's are vectors in the complex plane, the following equations can be established [23]:

$$\frac{R}{\cos\left(\left(\pi-\alpha\right)/2\right)}e^{i\left(\frac{\alpha}{2}-\beta\right)} - he^{i(\theta+\alpha-\beta)} - Re^{i(-\gamma)} = 2Re^{i\frac{\pi}{2}}$$
(11)

$$\gamma - \beta + \frac{\pi}{2} = \alpha. \tag{12}$$

Based on the above geometric relations, the web lengths  $L_1$ ,  $L_2$ , and  $L_3$  can be determined with the peeling angles  $\theta$  and  $\alpha$ . This web length and angle relationship is used for peeling speed estimation and control design.

The tension/strain dynamics can be obtained through mass conservation

$$\dot{l}_{1}\left(t\right) = \frac{v_{1}\left(t\right) - v_{p}\left(t\right)}{1 + \varepsilon_{1}\left(t\right)} \tag{13}$$

$$\dot{l}_{2}\left(t\right) = \frac{v_{p}\left(t\right)}{1+\varepsilon_{1}\left(t\right)} - \frac{v_{2}\left(t\right)}{1+\varepsilon_{2}\left(t\right)} \tag{14}$$

$$\dot{l}_{3}\left(t\right) = \frac{v_{p}\left(t\right)}{1+\varepsilon_{1}\left(t\right)} - \frac{v_{3}\left(t\right)}{1+\varepsilon_{3}\left(t\right)} \tag{15}$$

where  $l_i$  is the unstreched length of the web section with actual length  $L_i$  as in (8)–(10). The dynamic interactions among roller speed, tensions, angles, and adhesion variation can be described with the model introduced in this section.

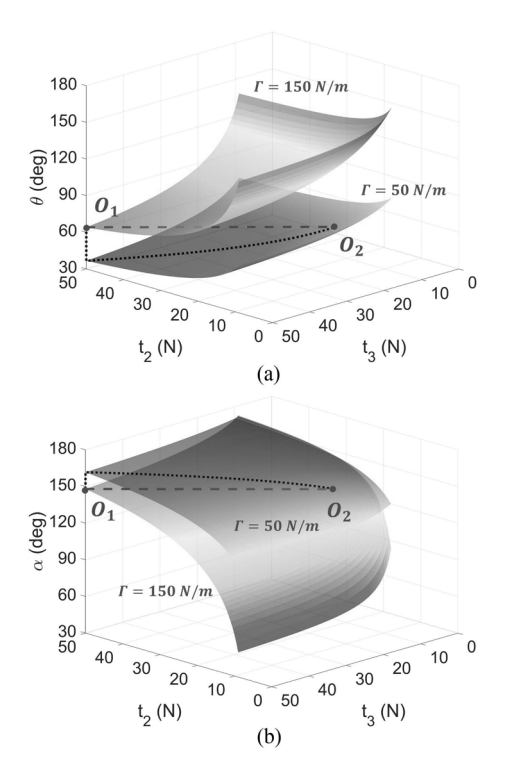


Fig. 2. Peeling with varying adhesion. (a)  $\theta$  as a function of  $t_2$ ,  $t_3$ . (b)  $\alpha$  as a function of  $t_2$ ,  $t_3$ .

### B. Effect of Adhesion Energy

Adhesion energy is a major factor that determines the tensions required to maintain a stable peeling process with the desired angles  $\theta_{\text{desired}}$  and  $\alpha_{\text{desired}}$ . Assuming steady-state peeling, (2), (6), and (7) can be used to show that  $t_1$  is entirely dependent on  $t_2$ ,  $t_3$ , and the adhesion energy  $\Gamma$ . Thus, for a given value of  $\Gamma$  at steady state,  $\theta$  and  $\alpha$  are purely functions of  $t_2$  and  $t_3$ . To understand the effect of adhesion energy on the peeling angles, a steady state analysis is conducted where the adhesion energy  $\Gamma$  is varied from 50 to 150 N·m and the peeling tensions  $t_2$  and  $t_3$  are varied from 10 to 50 N. Fig. 2 shows the response of the peeling angles as a function of both the peeling tensions and adhesion energy. Each of the two response surfaces in the figure corresponds to an adhesion energy level. The points on the surface represent equilibrium conditions for stable peeling. For example, consider a peeling process that begins at an operating point  $O_1$ on the surface corresponding to  $\Gamma$ = 150 N·m, and assume that the control goal is to maintain the same peeling angles, as it is throughout this article. If the adhesion energy changes to 50 N·m, the process condition will need to be changed to a point on the corresponding surface  $O_2$  through the adjustment of tensions  $t_2$ and  $t_3$ . This example demonstrates the need for a control strategy that accounts for adhesion energy variation while tracking the desired peeling angles in the R2R mechanical peeling process.

## III. CONTROL STRATEGY

The proposed control strategy is outlined in Fig. 3. It consists of a supervisory controller and two regulatory-level tension controllers. The supervisory controller takes the reference peeling

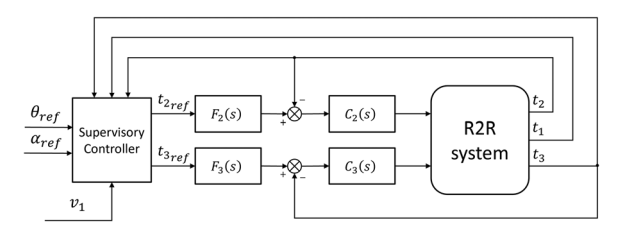


Fig. 3. Control loop block diagram.

angles  $\theta_{\rm ref}$  and  $\alpha_{\rm ref}$ , the tension measurements  $t_1$ ,  $t_2$ , and  $t_3$ , and the web speed  $v_1$  as inputs to estimate the instantaneous adhesion energy and the peeling front velocity. These estimates are then used to generate the tension setpoints  $t_{\rm 2ref}$  and  $t_{\rm 3ref}$  required to track the peeling angles  $\theta_{\rm ref}$  and  $\alpha_{\rm ref}$ . Then, the two regulatory-level tension controllers utilize both a feedforward  $F_i(s)$  and a feedback  $C_i(s)$  control block to track the tension setpoints from the supervisory controller using the motor torques on the two rewinding rollers as control inputs.

### A. Supervisory Control

As has been seen in Fig. 2, the peeling angles are determined by both the adhesion energy and peeling tensions. If the adhesion energy is known, then the reference peeling tensions  $t_{2ref}$  and  $t_{3\text{ref}}$  can be determined based on the reference angles  $\theta_{\text{ref}}$  and  $\alpha_{\rm ref}$ , which can then be used as the setpoints for the regulatory level tension controllers. However, the adhesion energy in the real peeling process is unknown and may vary. Thus, an online estimation of the adhesion energy is needed so that a feedback mechanism can be used to adjust the reference peeling tensions. To determine the adhesion energy on-line, it is necessary to first estimate  $v_p$ , as it determines whether the energy balance in (1) and (2) is in effect. When  $v_p$  is greater than zero, the films are peeling, which means that the adhesion energy,  $\Gamma$ , equals the energy release rate, G. When  $v_p$  equals zero, the films are not peeling apart, which means that G is smaller than  $\Gamma$ . Since the rate of change of the web length from the unwinding roller to the peeling front can be expressed as

$$\dot{L}_1 = v_1 - v_n. {16}$$

The peeling front velocity can be estimated numerically using the following discretized equation:

$$v_p^{(k)} = v_1^{(k)} - \frac{L_1(\theta^{(k)}, \alpha^{(k)}) - L_1(\theta^{(k-1)}, \alpha^{(k-1)})}{\Delta t}$$
(17)

where k is the discretized sample index and  $\Delta t$  is the time interval between samples. This estimation is updated at each time step to obtain the current peeling front velocity.

With the peeling front velocity estimation, the supervisory control algorithm can be developed as shown in Fig. 4. At each iteration, the peeling front velocity is estimated. If the estimated peeling front velocity  $v_p^{(k)}$  is greater than zero, which means the peeling occurs, the adhesion energy of the interface can be estimated using (1) and (2) by setting  $\Gamma_{\text{estimated}}^{(k)} = G^{(k)}$ . If  $v_p^{(k)}$  is zero, it means that the energy release rate  $G^{(k)}$  is less

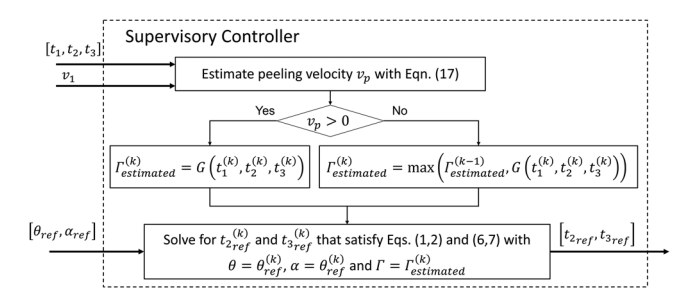


Fig. 4. Supervisory controller implementation.

than the adhesion energy  $\Gamma^{(k)}$ , i.e., no peeling is occurring. In this case, a new energy release rate  $G^{(k)'}$  is computed based on  $v_p^{(k)}=0$ . The estimated adhesion energy is set to be equal to the larger value between the adhesion energy estimation from the previous step  $\Gamma^{(k-1)}_{\rm estimated}$  and energy release rate  $G^{(k)'}$ . With the estimated adhesion energy, peeling tensions  $t_{\rm 2ref}^{(k)}$  and  $t_{\rm 3ref}^{(k)}$  can be computed using (1), (2), (6), and (7) to allow the peeling angles to follow  $\theta_{\rm ref}$  and  $\alpha_{\rm ref}$ .

### B. Peeling Tension Control

A tension dynamic model is considered for designing the regulatory level web tension controllers. The two webs between the peeling front and the rewinding rollers can be approximated as elastic springs with stiffnesses of  $K_i = \frac{A_i E_i}{L_i}$ . The tension dynamics are

$$\dot{t}_i = K_i (v_i - v_1) + w_i, \quad i = 2, 3$$
 (18)

where  $v_i$  is the web velocity at the rewinding roller and  $w_i$  is the disturbance caused by the difference between the peeling front velocity and the unwinding speed. When the peeling front velocity is the same as the unwinding velocity,  $w_i$  will be zero. The roller velocity dynamics can be described as [26]

$$\dot{v}_i = -\frac{f_i}{J_i}v_i - \frac{R_i^2}{J_i}t_i + \frac{R_i}{J_i}u_i, \quad i = 2, 3$$
 (19)

where  $f_i$  is the friction coefficient,  $J_i$  is the rotational inertia, and  $u_i$  is the motor torque applied on the *i*th rewinding roller.

The transfer function from the input torque to the tension output can be expressed as

$$P_{i}(s) = \frac{T_{i}(s)}{U_{i}(s)} = \frac{K_{i}R_{i}}{J_{i}s^{2} + f_{i}s + K_{i}R^{2}}$$
 (20)

Equation (20) represents the plant transfer function for the regulatory level tension controllers. A feedback controller  $C_i(s)$  can thus be designed to track the peeling tension as

$$C_i(s) = K_{P_i} + \frac{K_{I_i}}{s}. (21)$$

The closed loop transfer function can then be written as

$$G_{cl_{i}}(s) = \frac{K_{i}K_{P_{i}}R \cdot s + K_{i}K_{I_{i}}R}{J_{i}s^{3} + f_{i}s^{2} + (K_{i}R^{2} + K_{i}K_{P_{i}}R)s + K_{i}K_{I_{i}}R}.$$
(22)

Control gains  $K_{P_i}$  and  $K_{I_i}$  are chosen such that the characteristic polynomial in (22) can effectively reject the disturbance.

TABLE I
SYSTEM PARAMETERS

Parameters	Value
$E_1, E_2, E_3$	2.7 <i>GPa</i>
$R, R_1, R_2, R_3$	$0.0381 \ m$
$D_1$	$0.49 \ m$
$D_2$	1.02 m
$D_3$	1.59 m
$h_{w2}$ , $h_{w3}$	$127 \mu m$
b	$0.1016 \ m$
$J_2,J_3$	$0.9511 \ kg \cdot m^2$
$f_2$ , $f_3$	19.023 <i>N</i> ⋅ <i>s</i>
$K_{P_1}$ , $K_{P_2}$	14.38
$K_{I_1}$ , $K_{I_2}$	11.60
τ	0.05 s

To improve the tracking speed of the two tension controllers, a dynamic feedforward control scheme [27] is used. The purpose of the control design is to cancel the closed-loop poles and cancellable zeros to achieve unit feedback and fast closed-loop system performance. The transfer function of the feedforward block  $F_i(s)$  is given by

$$F_{i}(s) = \frac{J_{i}s^{3} + f_{i}s^{2} + (K_{i}R^{2} + K_{i}K_{P_{i}}R)s + K_{i}K_{I_{i}}R}{(\tau s + 1)^{2}(K_{i}K_{P_{i}}Rs + K_{i}K_{I_{i}}R)}.$$
(23)

Note that  $F_i(s)$  is the reciprocal of  $G_{cl_i}(s)$  with the filter term  $\frac{1}{(\tau s+1)^2}$  added so that it is not improper.

# IV. NUMERICAL SIMULATIONS AND EXPERIMENTAL VALIDATIONS

Both numerical simulations and experiments were conducted to validate the effectiveness of the proposed control strategy based on a R2R mechanical peeling testbed developed in house [23]. Table I gives the system parameters and controller parameters used in the article.

### A. Control System Architecture

The control system architecture of the R2R testbed is shown in Fig. 5. The controller utilizes both the real-time target and the FPGA target in a National Instrument CompactRIO. The FPGA target is used to perform sensor data acquisition, execute low-level signal processing, and generate output signals to the actuators. The motors driving the two rewinding rollers are integrated with quadrature encoders. The encoder speed interpolation is performed by counting the pulses at a rate of 1 MHz, and the speed reading is obtained at 1 kHz. To reduce the loadcell signal noise, a digital filter is implemented. The FPGA target generates both the pulse signal that activates the stepper motor attached to the unwinding roller and the voltage signals that control the brushless motors attached to the rewinding rollers. The real-time target implements the high-level control algorithm by interpreting the sensor measurements to produce the torque commands for the rewinding rollers. In addition, the real-time target carries out the data logging and visualization functions.

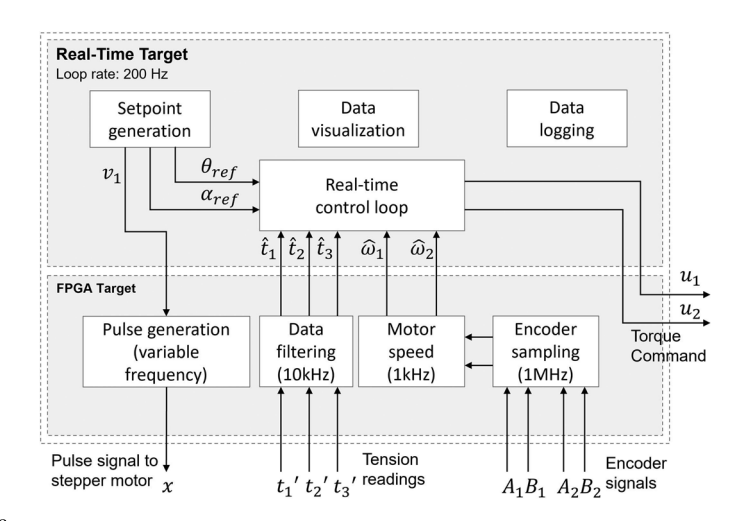


Fig. 5. Control system architecture.

# B. Simulation Study

Two simulation cases representing typical R2R mechanical peeling operations are considered in the article. The first has a constant adhesion energy  $\Gamma$  and changing reference peeling angles. This case could represent a situation where two substrates are being peeled with essentially constant adhesion energy between them, but it is desirable to change the peeling geometry to selectively transfer specific features or devices. The second case has a periodically varying  $\Gamma$  and constant reference peeling angles. This second case could represent a situation where there is an optimal peeling angle that needs to be maintained, but some pattern or physical process causes the adhesion energy to vary periodically. In the first case,  $\Gamma$  is fixed at 350 N·m. The unwinding speed is set as 0.0045 m/s to represent a start-up operating condition where the peeling angles need to be moved to their optimal point. At the beginning of the simulation, the peeling angles are maintained at  $\theta = 110^{\circ}$  and  $\alpha = 130^{\circ}$ . The setpoint  $\theta_{ref}$  is changed to 120° at time = 30 s and back to 110° at time = 70 s. The setpoint  $\alpha_{\rm ref}$  is changed to 140° at time = 50 s and back to  $130^{\circ}$  at time = 90 s. The simulation results are shown in Fig. 6. The dotted lines in Fig. 6(a) show the reference peeling angles and the solid lines show the resulting peeling angles. It is seen that the resulting peeling angles track the reference peeling angles closely. Fig. 6(b) shows that the peeling tensions are actively adjusted to track the peeling angles. Fig. 6(c) shows the adhesion energy and the instantaneous energy release rate. Changing the reference peeling angles affects both the tensions and energy release rate. For example, when the reference angle  $\theta_{\rm ref}$  is increased to 120° at time = 30 s, the energy release rate (G) drops below the adhesion energy ( $\Gamma$ ). As a result, the peeling front velocity drops to zero, as shown in Fig. 6(d). When the energy release rate is lower than the adhesion energy, the developed controller can adjust the peeling tensions such that the energy release rate is increased to catch up with the adhesion energy, and peeling is regained at the desired peeling angles.

In the second simulation case, the control objective is to maintain the peeling angles at  $\theta = 100^{\circ}$  and  $\alpha = 140^{\circ}$  while the adhesion energy varies periodically. The unwinding speed is set

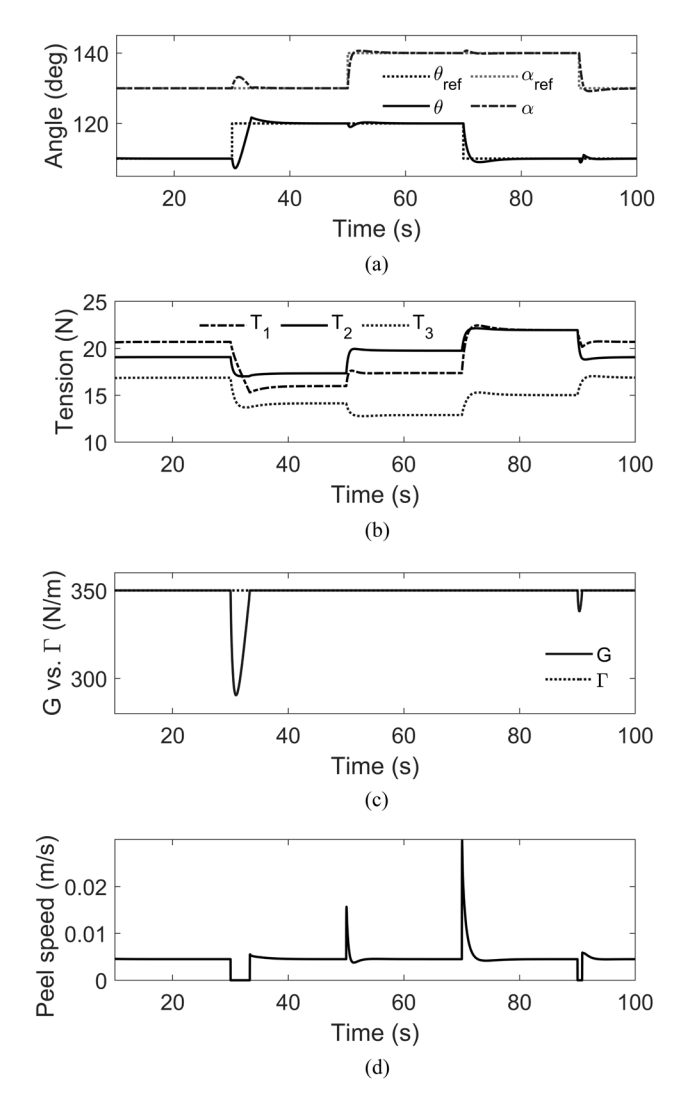


Fig. 6. Angle control numerical simulation results (case 1).

at 0.1 m/s to represent a steady state operating condition where the optimal peeling geometry needs to be maintained despite variation in other process parameters. The simulation results are shown in Fig. 7. The adhesion energy is set to vary between 110 and 80 N·m, with a period of 30 s, as shown in Fig. 7(a). As the adhesion energy changes, the peeling tensions change accordingly, as shown in Fig. 7(b). As a result, the peeling angles quickly converge to the reference angles, as shown in Fig. 7(c). At the transition points where the adhesion energy changes, the peeling angles deviate from the reference values due to the mismatch between the adhesion energy and the instantaneous energy release rate. When the adhesion energy increases, peeling angle  $\theta$  tends to increase and  $\alpha$  tends to decrease. Similarly, when the adhesion energy decreases, the peeling angle  $\theta$  tends to decrease and  $\alpha$  tends to increase. Both cases indicate that the peeling process is trying to transition into a new peeling front geometry to maintain peeling. However, the developed control algorithm can bring the angles back to the reference angles by actively controlling the tensions  $t_2$  and  $t_3$ , regardless of the adhesion energy change. Fig. 7(d) shows the peeling front velocity  $v_p$  in response to the adhesion energy changes. When

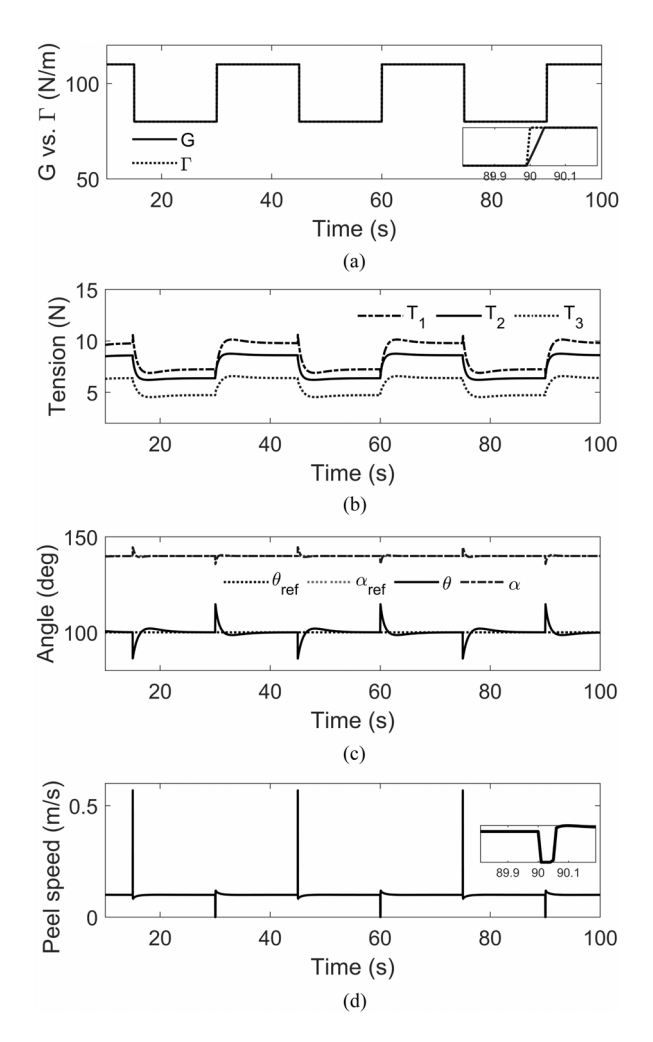


Fig. 7. Angle control numerical simulation results (case 2).

the adhesion energy  $\Gamma$  suddenly decreases, the energy release rate G will be larger than  $\Gamma$ , resulting in a sudden increase in the peeling front velocity. When the adhesion energy  $\Gamma$  suddenly increases, the energy release rate G will be smaller than  $\Gamma$  due to the delay in the tension controllers, as can be seen in the zoomed-in view in Fig. 7(a). This results in a sudden decrease of  $v_p$  to zero, as seen in Fig. 7(d), which means that no peeling is occurring during those transients.

The effectiveness of the dynamic feedforward in the regulatory level tension controller is demonstrated by comparing the performances of two different types of controllers, one with only proportional integral (PI) feedback and the other with PI feedback and the dynamic feedforward. The result is shown in Fig. 8. The tension setpoint for  $t_2$  is changed at 30 s and 40 s. It is shown that the tracking speed can be significantly improved, and the settling time reduced with the addition of the dynamic feedforward control.

# C. Experimental Validation

The angle control strategy developed in this article is tested with a sample prepared by laminating 3M Scotch heavy duty packaging tape (2 in wide) onto a polyethylene terephthalate

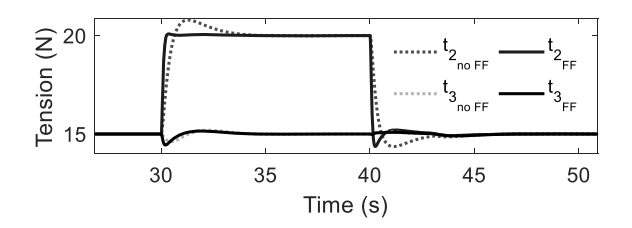


Fig. 8. Control performance comparison with and without the dynamic feedforward.

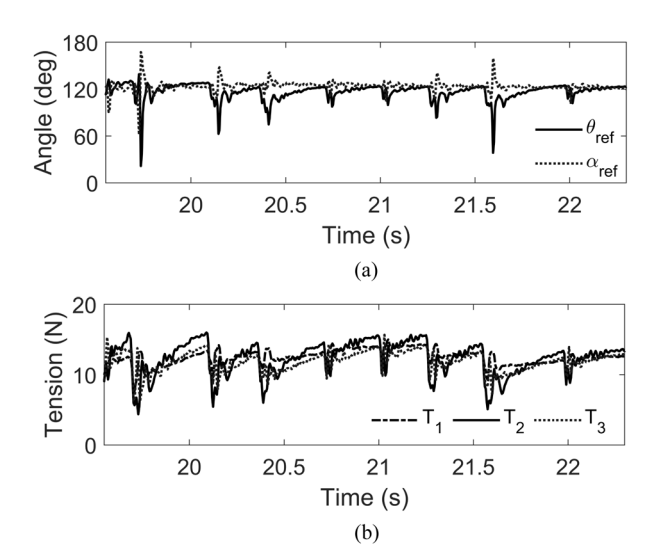


Fig. 9. Angle control experimental result (tracking  $120^\circ$ ). (a) Peeling angle. (b) Tension measurements.

(PET) film (0.005 in thick and 4 in wide). This sample was used because it could introduce a stick-slip phenomenon during peeling, where the adhesion energy between the tape and PET film changed periodically [29]. The stick-slip phenomenon causes the adhesion energy to change substantially during the peeling process, presenting a challenge for conventional web tension controllers to maintain the peeling angles, because they do not have an in-line estimator for the adhesion energy. The supervisory controller developed in this article is able to estimate the adhesion energy, based on which proper tension commands can be generated to maintain the proper peeling angles. The experimental result for peeling angle control using the supervisory controller is shown in Fig. 9. The unwinding speed was set at 0.012 m/s. Both reference peeling angles were set at  $\theta_{ref}$  $\alpha_{\rm ref} = 120^{\circ}$ . As shown in Fig. 9(a), the stick-slip phenomenon occurred during the peeling process. When it happened, there was a sudden decrease in  $\theta$  and increase in  $\alpha$ , forcing the angles to move toward their respective upper and lower bounds of  $0^{\circ}$  and 180°. However, these sudden changes only remained for a short period of time. With the peeling tensions actively controlled, as shown in Fig. 9(b), the peeling angles quickly recovered to the setpoint of 120°. Fig. 9(b) also shows that the peeling tensions were adjusted continuously during each stick-slip interval, even when the peeling angles were relatively stable. This was because the adhesion energy of the tape/PET interface increased throughout the stick-slip cycle and the peeling tensions were

actively adjusted to ensure continuous peeling with the reference peeling angles.

### V. CONCLUSION

A real-time supervisory control strategy is developed for a R2R dry transfer process using mechanical peeling for 2-D materials and printed electronics. The control strategy consists of a high-level supervisor controller and two regulatory level tension controllers. The supervisor controller utilizes a R2R peeling process model to estimate the peeling front velocity and the adhesion energy of the laminates being peeled. The estimates are then used to determine the peeling tension setpoints to track desired peeling angles. The regulatory level tension controllers utilize a PI feedback controller combined with a dynamic feedforward control to reduce the transient dynamics of the tension force. The developed control strategy allows active adjustment of the peeling tensions to achieve the desired tracking of peeling angles in real time. It enables the first ever capability to control transient behavior of a mechanical peeling process. The method is validated with both numerical simulation and experimental results and is expected to play an important role in ensuring the quality of dry transferred 2-D materials and printed electronics in large-scale R2R manufacturing.

### **A**CKNOWLEDGMENT

Any opinions, findings and conclusions or recommendations expressed in this material are those of the author(s) and do not necessarily reflect the views of the National Science Foundation.

### REFERENCES

- [1] T. Unander and H.-E. Nilsson, "Characterization of printed moisture sensors in packaging surveillance applications," *IEEE Sensors J.*, vol. 9, no. 8, pp. 922–928, Aug. 2009.
- [2] H. Kang et al., "Fully roll-to-roll gravure printable wireless (13.56 MHz) sensor-signage tags for smart packaging," Sci. Rep., vol. 4, 2014, Art no. 5387.
- [3] V. Subramanian, P. C. Chang, J. B. Lee, S. E. Molesa, and S. K. Volkman, "Printed organic transistors for ultra-low-cost RFID applications," *IEEE Trans. Compon. Packag. Technol.*, vol. 28, no. 4, pp. 742–747, Dec. 2005.
- [4] M. Allen, C. Lee, B. Ahn, T. Kololuoma, K. Shin, and S. Ko, "R2R gravure and inkjet printed RF resonant tag," *Micro-Electron. Eng.*, vol. 88, no. 11, pp. 3293–3299, 2011.
- [5] J. Noh et al., "Scalability of roll-to-roll gravure-printed electrodes on plastic foils," *IEEE Trans. Electron. Packag. Manuf.*, vol. 33, no. 4, pp. 275–283, Oct. 2010.
- [6] A. Gregg, L. York, and M. Strnad, "Roll-to-roll manufacturing of flexible displays," Flexible Flat Panel Displays, vol. 3, pp. 409–445, 2005.
- [7] P. Kopola et al., "Gravure printed flexible organic photovoltaic modules," Sol. Energy Mater. Sol. Cells, vol. 95, no. 5, pp. 1344–1347, 2011.
- [8] F. C. Krebs, S. A. Gevorgyan, and J. Alstrup, "A roll-to-roll process to flexible polymer solar cells: Model studies, manufacture and operational stability studies," *J. Mater. Chem.*, vol. 19, no. 30, 2009, Art no. 5442.
- [9] R. Søndergaard, M. Hösel, D. Angmo, T. T. Larsen-Olsen, and F. C. Krebs, "Roll-to-roll fabrication of polymer solar cells," *Mater. Today*, vol. 15, no. 1, pp. 36–49, 2012.
- [10] J. van den Brand, J. De Baets, T. Van Mol, and A. Dietzel, "Systems-in-foil-Devices, fabrication processes and reliability issues," *Micro-Electron. Rel.*, vol. 48, no. 8, pp. 1123–1128, 2008.
- [11] H. Xin, Q. Zhao, D. Chen, and W. Li, "Roll-to-roll mechanical peeling for dry transfer of chemical vapor deposition graphene," *J. Micro Nano-Manuf.*, vol. 6, no. 3, 2018, Art no. 031004.
- [12] Z. Qin, Z. Xu, and M. J. Buehler, "Peeling silicene from model silver substrates in molecular dynamics simulations," *J. Appl. Mech.*, vol. 82, no. 10, 2015, Art no. 101003.

- [13] S.-J. Yang, S. Choi, F. O. Odongo Ngome, K.-J. Kim, S.-Y. Choi, and C.-J. Kim, "All-dry transfer of graphene film by van der waals interactions," *Nano Lett.*, vol. 19, no. 6, pp. 3590–3596, 2019.
- [14] S. R. Na et al., "Clean graphene interfaces by selective dry transfer for large area silicon integration," *Nanoscale*, vol. 8, no. 14, pp. 7523–7533, 2016.
- [15] S. R. Na et al., "Selective mechanical transfer of graphene from seed copper foil using rate effects," ACS Nano, vol. 9, no. 2, pp. 1325–1335, 2015.
- [16] C. Linghu, S. Zhang, C. Wang, and J. Song, "Transfer printing techniques for flexible and stretchable inorganic electronics," *npj Flexible Electron.*, vol. 2, no. 1, p. 26, 2018, doi: 10.1038/s41528-018-0037-x.
- [17] X. Feng, M. A. Meitl, A. M. Bowen, Y. Huang, R. G. Nuzzo, and J. A. Rogers, "Competing fracture in kinetically controlled transfer printing," *Langmuir*, vol. 23, no. 25, pp. 12555–12560, 2007.
- [18] S. Cho, N. Kim, K. Song, and J. Lee, "Adhesiveless transfer printing of ultrathin microscale semiconductor materials by controlling the bending radius of an elastomeric stamp," *Langmuir*, vol. 32, no. 31, pp. 7951–7957, 2016.
- [19] M. A. Meitl et al., "Transfer printing by kinetic control of adhesion to an elastomeric stamp," *Nature Mater.*, vol. 5, no. 1, pp. 33–38, 2006.
- [20] B. Yoo, S. Cho, S. Seo, and J. Lee, "Elastomeric angled microflaps with reversible adhesion for transfer-printing semiconductor membranes onto dry surfaces," ACS Appl. Mater. Interfaces, vol. 6, no. 21, pp. 19247–19253, 2014.
- [21] H. Xin, R. Borduin, W. Jiang, K. M. Liechti, and W. Li, "Adhesion energy of as-grown graphene on copper foil with a blister test," *Carbon*, vol. 123, pp. 243–249, 2017.
- [22] Q. Zhao, N. Hong, D. Chen, and W. Li, "Controlling peeling front geometry in a roll-to-roll thin film transfer process," in *Proc. Int. Manuf. Sci. Eng. Conf.*, American Society of Mechanical Engineers, vol. 84256, 2020, p. V001T05A017.
- [23] Q. Zhao, N. Hong, D. Chen, and W. Li, "A dynamic system model for roll-to-roll dry transfer of two-dimensional materials and printed electronics," J. Dyn. Syst. Meas. Control, vol. 144, no. 7, 2022.
- [24] N. Hong, D. Kireev, Q. Zhao, D. Chen, D. Akinwande, and W. Li, "Roll-to-roll dry transfer of large-scale graphene," *Adv. Mater.*, vol. 34, no. 3, 2021, Art no. 2106615.
- [25] P. D. Mathur and W. C. Messner, "Controller development for a prototype high-speed low-tension tape transport," *IEEE Trans. Control Syst. Technol.*, vol. 6, no. 4, pp. 534–542, Jul. 1998, doi: 10.1109/87.701350.
- [26] P. R. Pagilla, N. B. Siraskar, and R. V. Dwivedula, "Decentralized control of web processing lines," *IEEE Trans. Control Syst. Technol.*, vol. 15, no. 1, pp. 106–117, Jan. 2007, doi: 10.1109/tcst.2006.883345.
- [27] M. Tomizuka, "Zero phase error tracking algorithm for digital control," J. Dyn. Syst. Meas. Control, vol. 109, no. 1, pp. 65–68, 1987.
- [28] N. Hong, Q. Zhao, D. Chen, K. M. Liechti, and W. Li, "A method to estimate adhesion energy of as-grown graphene in a roll-to-roll dry transfer process," *Carbon*, vol. 201, pp. 712–718, 2022.
- [29] M.-J. Dalbe, R. Villey, M. Ciccotti, S. Santucci, P.-P. Cortet, and L. Vanel, "Inertial and stick-slip regimes of unstable adhesive tape peeling," *Soft Matter*, vol. 12, no. 20, pp. 4537–4548, 2016.



**Qishen Zhao** received his B.S. degree in mechanical engineering from Shanghai Jiao Tong University, Shanghai, China. He obtained his Ph.D. degree in the mechanical engineering from the University of Texas at Austin, TX, USA, in 2022.

His research is focused on advanced manufacturing, mechatronics, dynamic system modeling and control, with application in roll-to-roll manufacturing systems.



Christopher Martin received the B.S. degree in mechanical engineering from the University of California Los Angeles, Los Angeles, CA, USA, in 2020. He is currently the Doctoral degree in dynamic systems and control with the Walker Department of Mechanical Engineering, University of Texas at Austin, Austin, TX, USA.

His current research focus is on optimal and robust control, specifically regarding highly non-linear or switched systems.



Nan Hong (Member, IEEE) received the Ph.D. degree from the Walker Department of Mechanical Engineering, University of Texas at Austin, Austin, TX, USA, in 2022.

His current research interests include the process study of roll-to-roll graphene dry transfer and its application.



**Dongmei Chen** (Member, IEEE) received the Ph.D. degrees in mechanical engineering from the University of Michigan, Ann Arbor, MI, USA, in 2006.

She is currently a Professor with the Walker Department of Mechanical Engineering, University of Texas at Austin, Austin, TX, USA. Her current research interests include theories of switching control, optimal control, and reduced order modeling, with applications in energy systems.

Dr. Chen is a recipient of CAREER award from the National Science Foundation in 2011 and the 2016 IEEE PES Prize Paper Award.



**Wei Li** received the Ph.D. degree in mechanical engineering from the University of Michigan, Ann Arbor, MI, USA, in 1999.

He is currently a Professor of mechanical engineering with the Walker Department of Mechanical Engineering, University of Texas at Austin, Austin TX, USA. His research interests include nano and biomaterials processing and manufacturing, including the growth and transfer of two-dimensional materials, biomedical device design and manufacturing, and monitoring, di-

agnosis, and control of manufacturing processes.